Acta Crystallographica Section D
Biological Crystallography
ISSN 0907-4449

Structure of the polypeptide crotamine from the Brazilian rattlesnake *Crotalus durissus terrificus*

Monika A. Coronado,[a,b] Azat Gabdulkhakov,[c] Dessislava Georgieva,[b] Banumathi Sankaran,[d] Mario T. Murakami,[e] Raghuvir K. Arni[a] and Christian Betzel[b]*

[a]Multi User Center for Biomolecular Innovation, Department of Physics, São Paulo State University, UNESP/IBILCE, C. Postal 136, 15054-000 São José do Rio Preto-SP, Brazil, [b]Institute of Biochemistry and Molecular Biology, Hamburg University, Martin-Luther-King Platz 6, 20146 Hamburg, Germany, [c]Institute of Protein Research, RAS, Pushchino, Moscow Region 142290, Russian Federation, [d]Physical Biosciences Division, Lawrence Berkeley National Laboratory, 1 Cyclotron Road, Berkeley, CA 94702, USA, and [e]Biosciences National Laboratory, National Center for Energy and Materials Research, Giuseppe Maximo Scolfaro 10000, 13083-970 Campinas-SP, Brazil

Correspondence e-mail: christian.betzel@uni-hamburg.de

Received 27 April 2013
Accepted 29 June 2013

PDB Reference: crotamine, 4gv5

The crystal structure of the myotoxic, cell-penetrating, basic polypeptide crotamine isolated from the venom of *Crotalus durissus terrificus* has been determined by single-wavelength anomalous dispersion techniques and refined at 1.7 Å resolution. The structure reveals distinct cationic and hydrophobic surface regions that are located on opposite sides of the molecule. This surface-charge distribution indicates its possible mode of interaction with negatively charged phospholipids and other molecular targets to account for its diverse pharmacological activities. Although the sequence identity between crotamine and human β-defensins is low, the three-dimensional structures of these functionally related peptides are similar. Since crotamine is a leading member of a large family of myotoxic peptides, its structure will provide a basis for the design of novel cell-penetrating molecules.

1. Introduction

Crotamine, a highly basic (pI = 10.3) 42-amino-acid polypeptide (molecular mass 4.8 kDa), was first isolated in 1947 from the venom of the Brazilian rattlesnake *Crotalus durissus terrificus* (Gonçalves & Polson, 1947). Crotamine is of high pharmacological importance as a potent analgesic and has been shown to be over 30-fold more effective than morphine (Giorgi *et al.*, 1993; Mancin *et al.*, 1998). It also selectively inhibits and interferes with the functioning of $K_v1.3$ channels, promotes the permeability of bacterial membranes (Oguiura *et al.*, 2011) and is considered to be a promising cell-penetrating agent capable of accumulating in the nucleus and in transporting DNA into replicating cells (Kerkis *et al.*, 2004, 2010). It has been suggested that crotamine possesses the potential to transport drugs into mammalian cells without requiring specific receptors. More recently, it has been demonstrated that crotamine possesses both antitumoral and antibacterial activities (Lee *et al.*, 2011).

Crotamine possesses three disulfide bridges (Boni-Mitake *et al.*, 2001) and a number of isoforms have been characterized (Toyama *et al.*, 2000; Ponce-Soto *et al.*, 2007). The overall fold of crotamine is homologous to antimicrobial peptides (AMPs) belonging to the α-defensin, β-defensin and insect defensin families (Dimarcq *et al.*, 1998) and possessing the same number of disulfide bridges (Hoover *et al.*, 2001). Despite the differences in amino-acid composition, crotamine possesses the same structural scaffold as mammalian α-defensins and β-defensins, consisting of a three-stranded β-sheet core and a framework of loops stabilized by six disulfide-linked cysteines (Ganz *et al.*, 1985). Both α-defensins and β-defensins consist of a triple-stranded β-sheet with a distinct 'defensin' fold (Ganz, 2003). Functionally, defensins display a wide spectrum of activities and trigger diverse effects. Some of these peptides

Table 1
Crystal parameters and data-collection and refinement statistics.

Values in parentheses are for the highest resolution shell.

	Pt-derivative	Native
Data collection		
Beamline	X12, DORIS III	P14, PETRA III
Space group	$I2_12_12_1$	$I2_12_12_1$
Unit-cell parameters (Å)	a = 66.94, b = 74.55, c = 80.45	a = 66.92, b = 74.33, c = 80.19
Resolution (Å)	54.6–2.5 (2.60–2.50)	54.5–1.7 (1.79–1.69)
Measured reflections	36251 (1931)	139383 (13889)
Completeness (%)	99.4 (75.2)	97.7 (85.3)
Averaged multiplicity	5.3 (2.5)	6.3 (5.0)
Average $I/\sigma(I)$	26.0 (5.7)	20.8 (1.1)
$R_{\rm merge}$† (%)	3.6 (16.7)	3.7 (14.2)
Structure solution (*AutoSol*)		
No. of sites	3	
Skew‡	0.16	
$CORR_{r.m.s.}$§	0.88	
Figure of merit (FOM)	0.36	
Estimated map CC	0.56	
Structure building (*AutoBuild*)		
Residues built	99	
$R_{\rm work}$ (%)	33.1	
$R_{\rm free}$ (%)	37.3	
Map CC	0.75	
Refinement		
Resolution (Å)		10.0–1.7
R factor (%)		16.6 (17.1)
Free R factor (%)		22.5 (22.9)
Overall B factor (Å^2)		33.3
R.m.s. deviations		
Bond lengths (Å)		0.03
Bond angles (°)		2.85
Ramachandran plot, residues in (%)		
Most favoured region		95.8
Additionally allowed region		4.2
No. of molecules		
Protein		3
Water		65
Sulfate ions		3
Thiocyanate ions		4
Glycerol		4

† $R_{\rm merge} = \sum_{hkl}\sum_i |I_i(hkl) - \langle I(hkl)\rangle| / \sum_{hkl}\sum_i I_i(hkl)$, where $\langle I(hkl)\rangle$ is the mean intensity of the observations $I_i(hkl)$ of reflection hkl. ‡ Deviation from a Gaussian distribution. § Correlation of a local r.m.s. density.

possess anti-Gram-positive activities and participate in antibacterial defence reactions (Cociancich *et al.*, 1993).

Although crotamine was isolated more than 60 years ago (Gonçalves & Polson, 1947), it has been extremely recalcitrant to crystallization, probably owing to its high intrinsic flexibility as confirmed by NMR studies (Endo *et al.*, 1989; Nicastro *et al.*, 2003; Fadel *et al.*, 2005).

In this work, we report the first crystal structure of crotamine, a leading member of a large family of highly basic polypeptides.

2. Material and methods

2.1. Purification of crotamine

The purification and crystallization of crotamine have been described before (Coronado *et al.*, 2012). In summary, crotamine from crude *C. durissus terrificus* venom obtained from CEVAP (Center for the Study of Venoms and Venomous Animals), Botucatu, Brazil was isolated by a single cation-exchange chromatography step applying a MonoS HR 10/10 column (Amersham Biosciences). The molecular mass and sequence of the amino acids were analysed by mass spectroscopy and single crystals suitable for X-ray diffraction data collection were obtained after 2 d by vapour diffusion when crotamine at a concentration of 22 mg ml^{-1} in deionized water was equilibrated against a reservoir solution consisting of 0.2 *M* sodium thiocyanate, 1.9 *M* ammonium sulfate pH 6.1, as described in detail previously (Coronado *et al.*, 2012).

2.2. X-ray data collection

Since attempts to solve the structure of crotamine by molecular replacement using either the NMR-derived coordinates of crotamine (PDB entries 1h5o and 1z99; Nicastro *et al.*, 2003; Fadel *et al.*, 2005) or the defensin structures known to date were unsuccessful, SAD (single-wavelength anomalous dispersion) was applied to solve the phase problem. A native data set was collected to 1.7 Å resolution on the EMBL beamline P14 at PETRA III (DESY/Hamburg). The native X-ray diffraction data were integrated, processed and scaled using the *XDS* software (Kabsch, 2010). A suitable heavy-metal derivative was obtained by soaking crystals for approximately 12 h in a 0.1 *M* potassium hexachloroplatinate (K_2PtCl_6) solution (Heavy Atom Screens; Hampton Research). Prior to data collection, crystals were flash-cooled in a nitrogen-gas stream at 100 K. MAD (multi-wavelength anomalous dispersion) data were collected on the EMBL beamline X12 at DORIS III (DESY/Hamburg) at the peak, inflection and high-energy points of the Pt fluorescence spectrum. However, the data from the peak wavelength displayed a very clear anomalous signal and the SAD technique was used. Anomalous data reduction and determination of the space group and unit-cell parameters were carried out with the *iMOSFLM* software (Battye *et al.*, 2011). The data-collection statistics are presented in Table 1.

2.3. Model building and refinement

Phases were determined by SAD using the program *Phaser* in the *PHENIX* software suite (Adams *et al.*, 2010) at 2.5 Å resolution by exploiting the anomalous signal of platinum ions. The initial electron-density map was of sufficient quality to build approximately 90% of three polypeptide chains of crotamine present in the asymmetric unit using automated building in *phenix.autobuild* (Adams *et al.*, 2010). *REFMAC* (Murshudov *et al.*, 2011) in combination with the inspection of the electron-density maps using the program *Coot* (Emsley *et al.*, 2010) was used to complete and refine the model to 1.7 Å resolution with an R value of 16.6% and an $R_{\rm free}$ of 22.5%. The final model also contains 65 solvent water molecules, four glycerol molecules, four thiocyanate ions and three sulfate ions. Refinement statistics are presented in Table 1.

2.4. Small-angle X-ray scattering (SAXS)

Crotamine samples were prepared in conditions with different pH values: (i) 0.05 *M* acetic acid pH 5.0, (ii) 0.05 *M*

Tris–HCl pH 9.0 and (iii) pure water. SAXS data were collected with concentrations of 1, 2, 5 and 9.7 mg ml^{-1}. The concentrations were determined at 280 nm using a NanoDrop 2000C spectrophotometer. The extinction coefficient of the protein was calculated using the online program *ProtParam* (Gasteiger *et al.*, 2005). SAXS data from crotamine solutions were collected on EMBL beamline P12 at PETRA III (DESY/Hamburg) at 295 K using a two-dimensional photon-counting PILATUS 2M pixel X-ray detector (DECTRIS). All data sets were normalized to the incident-beam intensity and corrected for detector response, and scattering of the buffer was subtracted using *ATSAS* (Petoukhov *et al.*, 2007).

Table 2
Hydrogen-bond contacts of crotamine molecules in the asymmetric unit.

A	*B*	*C*	Distance (Å)
Glu15 OE1	Lys35 NZ		3.27
Glu15 OE1	Cys18 N		2.91
Asp24 O	Lys14 NZ		3.11
Lys35 NZ	Glu15 OE1		2.95
Cys18 N	Glu15 OE1		2.89
Lys14 NZ	Pro21 O		3.00
Lys14 NZ	Asp24 O		2.79
	Cys11 O	Arg31 NH1	2.82
	Cys11 O	Arg31 NH2	2.97
	Arg31 NH2	Tyr1 OH	2.64

3. Results and discussion

3.1. Overall structure

Crystals of crotamine belonged to space group $I2_12_12_1$, with unit-cell parameters a = 66.92, b = 74.33, c = 80.19 Å, and contained three molecules in the asymmetric unit. The overall fold of crotamine is illustrated in Fig. 1(*a*). Residues Lys2–Lys7 form a single α-helical turn which flanks a two-stranded antiparallel β-sheet formed by residues Gly9–Pro13 (β1) and Trp34–Lys38 (β2) located in the core of the molecule. A short α-helical turn is formed by residues Pro20–Ser23. The polypeptide is stabilized by three disulfide bonds: Cys4–Cys36, Cys11–Cys30 and Cys18–Cys37. The disulfide bridge Cys4–Cys36 anchors the first α-helical segment to β2. β1 and α2 are connected by a flexible loop Lys14–Leu19, and helical turn α2 is connected to β2 by a more extended and flexible loop formed by residues Asp24–Arg33. Overall, the topology can be classified as $\alpha1\beta1\alpha2\beta2$. The β-sheet is stabilized by hydrogen bonds between strands β1 and β2, involving residues His10–Cys37 and Phe12–Lys35, and hydrogen bonds between strand β2 and α2, formed by Ser23–Lys38. Two hydrogen bonds connect β2 to the C-terminal β-turn.

As crotamine is relatively small, all charged as well as hydrophobic residues are exposed to the solvent, a circumstance that makes crotamine unusually 'sticky'. It is likely that these electrostatic and hydrophobic forces on the surface, in combination with a disulfide-stabilized molecular scaffold, enable crotamine or crotamine oligomers to complex with target proteins. Most hydrophobic residues are located on one side of the molecule and the positively charged residues Lys2, Lys6, Lys7, Lys14, Lys16, Lys27, Lys35, Lys38, Lys39, Arg31 and Arg33 are clustered on the opposite side, as shown in Fig. 1(*b*). These residues are exposed on the surface of crotamine and form distinct hydrophobic and cationic regions which are positioned roughly on opposite sides of the amphiphilic molecule, as shown in Fig. 1(*c*).

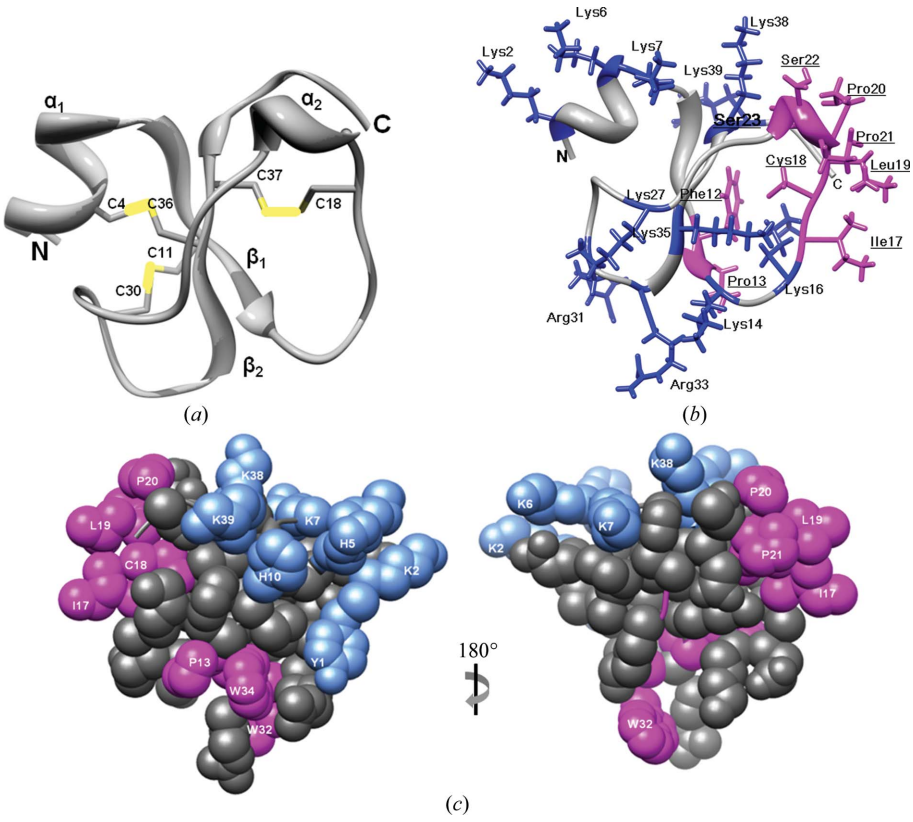

Figure 1
(*a*) Structure of crotamine. The N- and C-termini and the cysteine residues are labelled. (*b*) The highly hydrophobic residues in pink are located on one side of the molecule and the positively charged residues in blue are on the opposite side. (*c*) Space-filling presentation of crotamine, highlighting the well defined amphipathic surface region in blue and pink.

Superposition with the crotamine NMR structure (Nicastro *et al.*, 2003; Fadel *et al.*, 2005) resulted in a mean C^{α} r.m.s.d. value of 2.12 Å, indicating a relatively high spatial deviation between the NMR and crystal structures, and higher flexibility of the NMR solution structure.

3.2. The quaternary arrangement

Both SAXS and dynamic light-scattering measurements indicated that the protein was monomeric in solution (Coronado *et al.*, 2012). In the crystal structure three molecules of crotamine

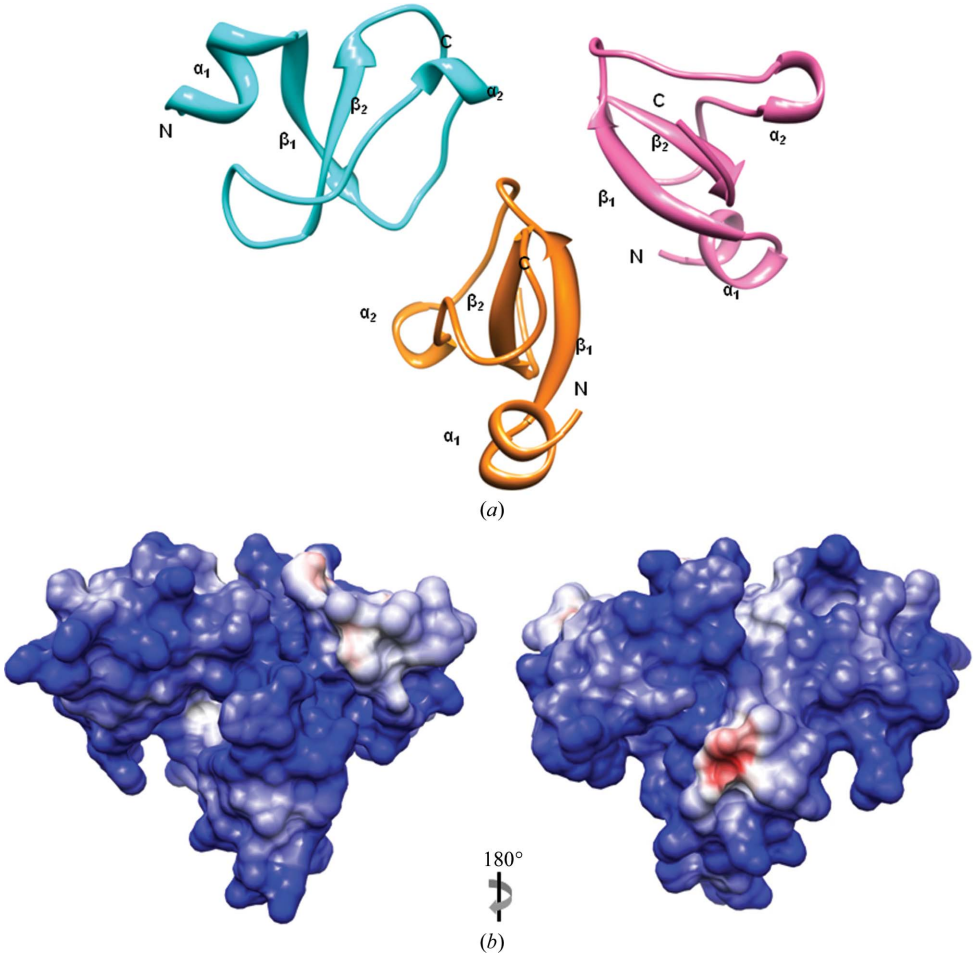

Figure 2
(*a*) Cartoon plot of the crotamine trimer. (*b*) Surface-charge distribution in two orientations.

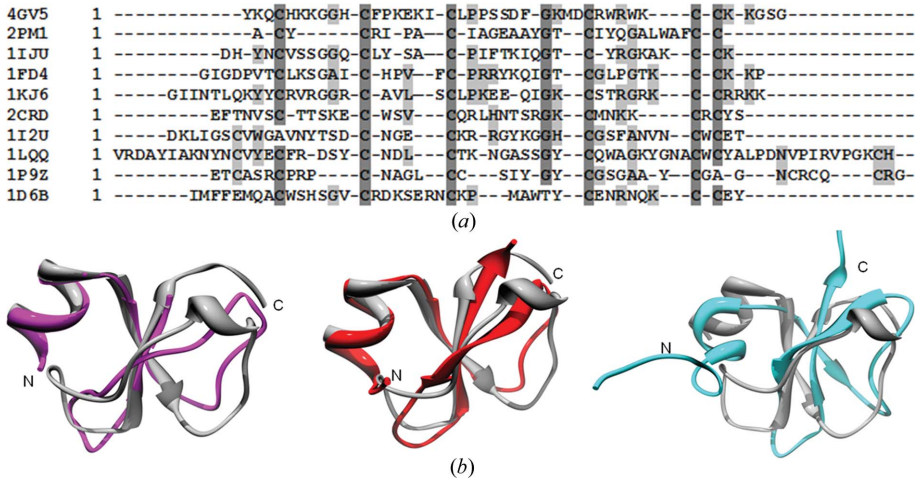

Figure 3
(*a*) Sequence alignment of antimicrobial peptides. Conserved Cys residues are indicated in dark grey. Crotamine (PDB entry 4gv5), defensin-like peptide 2 (PDB entry 1d6b), heliomicin (PDB entry 1i2u), toxin III (PDB entry 1lqq), *Eucommia* antifungal peptide 2 (PDB entry 1p9z), charybdotoxin (PDB entry 2crd), human β-defensin 1 (PDB entry 1iju), human β-defensin 2 (PDB entry 1fd4), human β-defensin 3 (PDB entry 1kj6) and human α-defensin 1 (PDB entry 2pm1). (*b*) Superposition of crotamine (cartoon plot in light grey) with hβD-1 (PDB entry 1iju, pink), hβD-2 (PDB entry 1fd4, red) and hβD-3 (PDB entry 1kj6, cyan). The corresponding C^{α} r.m.s.d. values are 1.8, 1.8 and 2.6 Å, respectively.

are present in the asymmetric unit (Fig. 2), which is stabilized by a number of intermolecular contacts involving main-chain and side-chain atoms. In the crystal structure chains *A*–*B*, *A*–*C* and *B*–*C* bury 353, 261 and 121 Å^2, respectively. This corresponds to approximately 6–10% of the overall surface area of each monomer. A careful inspection of interactions stabilizing the trimer in the crystal showed the presence of two sulfate ions in the interface of chains *A* and *C*, close to residues Cys11 and His10 of chain *C* and Lys16, Phe12 and Pro13 of chain *A*. In addition, four glycerol and three thiocyanate molecules were identified at almost equivalent positions in the interface regions of chains *A*–*B*, *B*–*C* and *C*–*A*, forming hydrogen-bonding, van der Waals and hydrophobic interactions stabilizing the trimer. All intermolecular interactions are summarized in Table 2.

3.3. Structural similarities between crotamine and antimicrobial peptides

The high positively charged surface permits us to hypothesize that crotamine can interact electrostatically with the negatively charged surface of membranes with the potential to induce the formation of gaps, through which ions and/or other molecules can diffuse.

In Fig. 3(*a*) and Table 3 a sequence comparison and structural characteristics of homologous antimicrobial (AMP) and antimicrobial-like (defensin-like) peptides of different origin are shown. The defensin-like polypeptides share relatively low sequence identities in the range 15–35%; however, they have a homologous secondary-structural arrangement of α-helices, β-sheets and random coils, as well as the conservation of six cysteine residues forming three disulfide

Table 3
Comparison of the amino-acid sequence of crotamine with α-defensin, β-defensin and defensin-like peptides.

Amino-acid sequences are given in one-letter code.

AMP	Length	Amino-acid sequence	Secondary structure	Disulfide bridges	Organism	PDB code
CRO	42	YKQCHKKGGHCFPKEKICLPPSSDFGKMDCRWR-WKCCKKGSG	α-Helix aligned to antiparallel two-stranded β-sheet	3	*Crotalus durissus terrificus*	4gv5
EAFP-2	30–43	ETCASRCPRPCNAGLCCSIYGYCGSGAAYCGAGN-CRCQCRG	Two α-helices aligned to three-stranded β-sheet random coils	5	*Eucommia ulmoide*	1p9z
CHTX	30–40	EFTNVSCTTSKECWSVCQRLHNTSRGKCMNKKC-RCYS	Small three-strand β-sheet, α-helix, random coil	3	*Leiurus quinquestriatus hebraeus*	2crd
HEL	44	DKLIGSCVWGAVNYTSDCNGECKRRGYKGGHC-GSFANVNCWCET	α-Helix, three-stranded antiparallel β-sheet, random coil	3	*Heliothis virescen*	1i2u
Toxin III	64	VRDAYIAKNYNCVYECFRDSYCNDLCTKNGASS-GYCQWAGKYGNACWCYALPDNVPIRVPGKCH	α-Helix, three-stranded antiparallel β-sheet, random coil	4	*Leiurus quinquestriatus hebraeus*	1lqq
DLP-2	42	IMFFEMQACWSHSGVCRDKSERNCKPMAWTYCE-NRNQKCCEY	Small α-helix, two-stranded β-sheet, random coils	3	*Ornithorhynchus anatinus*	1d6b
HβD-1	36	DHYNCVSSGGQCLYSACPIFTKIQGTCYRGKAK-CCK	α-Helix, three-stranded β-sheet, random coils	3	*Homo sapiens*	1iju
HβD-2	41	GIGDPVTCLKSGAICHPVFCPRRYKQIGTCGLPGT-KCCKKP	α-Helix, three-stranded β-sheet, random coils	3	*Homo sapiens*	1fd4
HβD-3	45	GIINTLQKYYCRVRGGRCAVLSCLPKEEQIGKCS-TRGRKCCRRKK	α-Helix, three-stranded β-sheet, random coils	3	*Homo sapiens*	1kj6
HNP-1	30	ACYCRIPACIAGERAAYGTCIYQGRLWAFCC	Three-stranded β-sheet, random coils	3	*Homo sapiens*	2pm1

Table 4
Summary of charged and hydrophobic residues of crotamine in comparison to other antimicrobial peptides.

SA: total surface accessibility.

	CRO	HβD-1	HβD-2	HβD-3	CHTX	DLP-2	HEL	Toxin III	HNP-1	EAFP-2
Arg^+	2	1	2	7	3	3	2	3	1	4
Asp^-	2	1	1	—	—	1	2	4	—	—
Glu^-	1	—	—	2	2	4	2	1	1	1
Lys^+	9	4	5	6	4	3	3	4	—	—
Total	14	6	8	15	9	11	9	12	2	5
Positive	11	5	7	13	7	6	5	7	1	4
Negative	3	1	1	2	2	5	4	5	1	1
Trp	2	—	—	—	1	2	2	2	1	—
Tyr	1	3	1	—	1	2	2	7	3	3
Phe	2	1	1	—	1	2	1	1	1	—
SA (Å^2)	3223	2808	2858	4025	3019	3888	3060	4069	2246	2997

bonds (Schibli *et al.*, 2002). An overall structural comparison of the three known human defensin structures hβD-1, hβD-2 and hβD-3 with crotamine is shown in Fig. 3(*b*). The corresponding C^α r.m.s.d. values are 1.8, 1.8 and 2.6 Å, respectively. It is obvious that, despite the moderate sequence identity, evolutionary selective pressures have favoured a similar overall three-dimensional structure and fold of these functionally related peptides. The predominance of functionally relevant positively charged residues (Table 4) is a common feature of crotamine and defensins. Most probably this facilitates the electrostatic interactions with the anionic membrane surface.

Despite high overall structural conservation, some physicochemical differences between human β-defensins and crotamine have been addressed as likely determinants of the observed functional differences (Yount *et al.*, 2009). The arginine and lysine content varies between the three human β-defensins and crotamine, as shown in Table 4. These distributions of charged residues are also typical for β-defensins from other animals. In contrast, lysine residues are relatively rare in α-defensins. The predominance of positively charged residues in crotamine is likely to facilitate electrostatic interactions with the anionic membrane surface. The total surface accessibility of crotamine and hβDs differs, the accessible surface area changes occur when residues on the molecule surface are replaced by others having large or smaller side chains (Table 4). The α-helix, the antiparallel β-sheet and the β-turn present in the human β-defensins 1–3 (Hoover *et al.*, 2000, 2001; Schibli *et al.*, 2002) are also conserved in crotamine.

Fig. 4 is an overview highlighting the structural similarities and differences of defensin-like polypeptides. In all structures the basic secondary-structural elements and disulfide bridges, a feature initially attributed to polypeptides classified as defensins, are conserved. However, toxin III and *Eucommia* antifungal peptide 2 (EAFP-2) have four and five disulfide bonds, respectively. Among the antimicrobial polypeptides with six cysteines the α-defensin and β-defensin group is the best characterized to date. They are widely distributed in different phyla, including plants, insects, arthropods and vertebrates (Ganz, 2004; Lehrer *et al.*, 1993). The polypeptide defensin-like peptide 2 (DLP-2) isolated from platypus (*Ornithorhynchus anatinus*) venom (Torres *et al.*, 2000) shares 34% sequence identity with crotamine but displays no antimicrobial activity. Heliomicin (HEL), which is known to be an

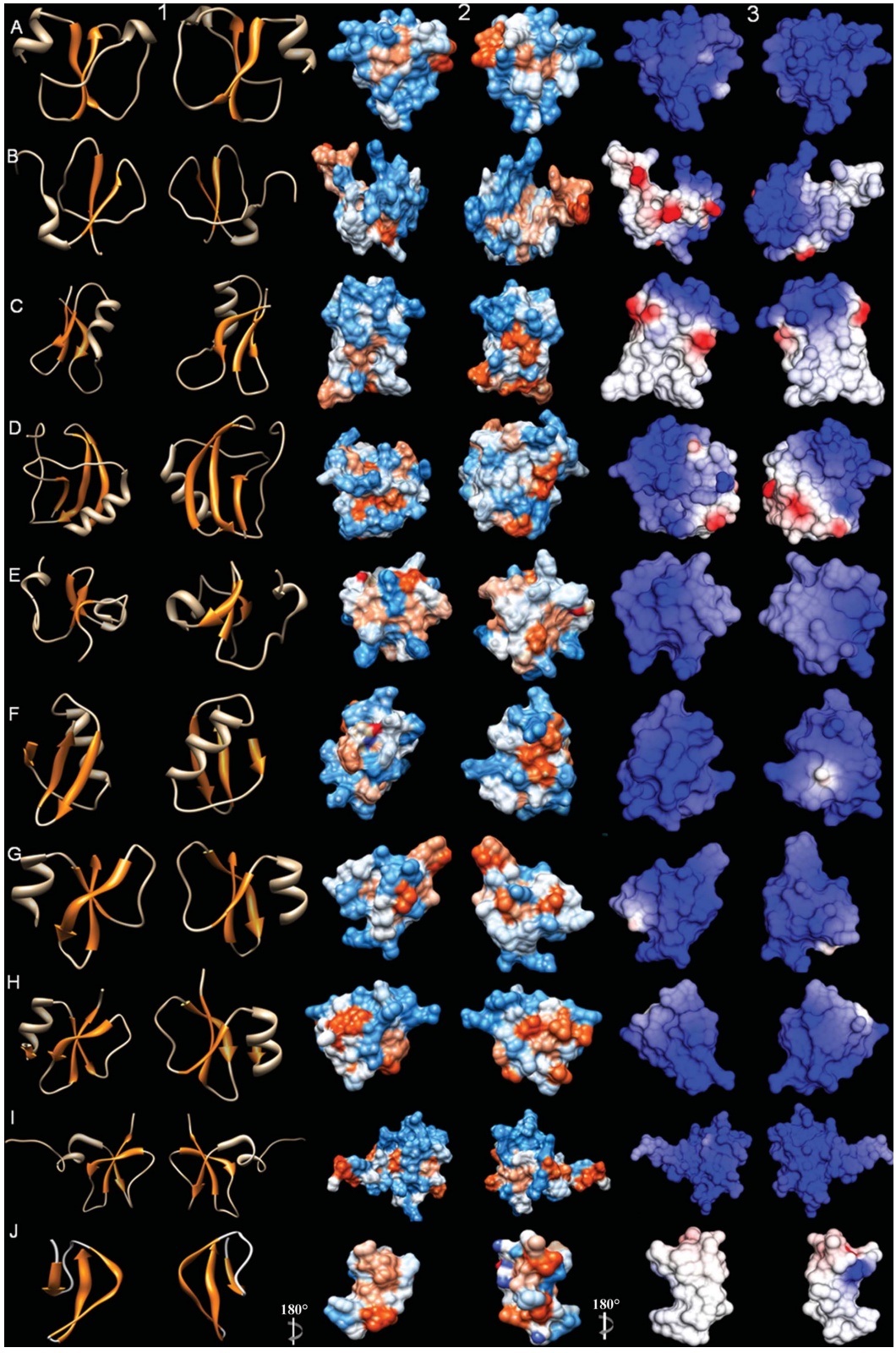

Figure 4
Structure comparison of crotamine with homologous antimicrobial and antimicrobial-like peptides from different organisms in two orientations. Column 1, the γ-core domain is shown in orange. Column 2, hydropathy plot overlay: dark orange/hydrophobic; light orange/intermediate; blue/hydrophilic. Column 3, surface charge: blue, basic (Arg, Lys); red, acidic (Asp, Glu). Row A, crotamine from *C. durissus terrificus* venom (PDB entry 4gv5); row B, defensin-like peptide 2 (1d6b); row C, heliomicin (1i2u); row D, toxin III (1lqq); row E, *Eucommia* antifungal peptide 2 (1p9z); Row F, charybdotoxin (2crd); row G, human β-defensin 1 (1iju); row H, human β-defensin 2 (1fd4); row I, human β-defensin 3 (1kj6); row J, human α-defensin 1 (2pm1).

antifungal defensin from the lepidopteran *Heliothis virescens* (Lamberty *et al.*, 2001; Sverdlova & Nefelova, 1999), contains two Arg and three Lys residues and shares 22% sequence identity with crotamine. Insect defensins are characterized by a cysteine-stabilized $\alpha\beta$ motif (CS$\alpha\beta$), which consists of an α-helix and an antiparallel triple-stranded β-sheet connected by two disulfide bridges (Lamberty *et al.*, 2001; Cornet *et al.*, 1995). The CS$\alpha\beta$ motif has also been encountered in the scorpion toxin charybdotoxin (CHTX; Bontems *et al.*, 1992), toxin III (Landon *et al.*, 1996) and in plant defensins such as EAFP-2 (Huang *et al.*, 2004; Carvalho & Gomes, 2009). This motif has not been observed in snake-venom toxin to date. The structure of charybdotoxin, a peptide from the venom of the yellow scorpion *Leiurus quinquestriatus hebraeus* that affects K^+ channels, shares approximately 15% sequence similarity with crotamine.

In conclusion, the high-resolution crystal structure of crotamine shows an asymmetric surface-charge distribution which corresponds to the observed activity. The crystal structure of crotamine will also help to understand the mode of action of other homologous peptides such as myotoxin and will support the design of novel molecules capable of transporting drugs into cells.

This project was supported by grants from the Deutsche Forschungsgemeinschaft (Project BE 1443-18-1, 26-1), FAPESP, CNPq, CAPES and DAAD (PROBAL 50754442). MAC thanks CAPES (grant NR-8248/12-5) for the exchange fellowship. DG thanks the Alexander von Humboldt Foundation (AvH), Bonn, Germany for providing a Research Fellowship. The Berkeley Center for Structural Biology is supported in part by the National Institutes of Health, National Institute of General Medical Sciences and the Howard Hughes Medical Institute. The Advanced Light Source is supported by the US Department of Energy under Contract No. DE-AC02-05CH11231. We would like to thank Dr Alexey Kikhney and the staff of the Biological Small Angle Scattering group (EMBL/Hamburg, Germany) for providing the opportunity to perform SAXS measurements.

References

Adams, P. D. *et al.* (2010). *Acta Cryst.* D**66**, 213–221.

Battye, T. G. G., Kontogiannis, L., Johnson, O., Powell, H. R. & Leslie, A. G. W. (2011). *Acta Cryst.* D**67**, 271–281.

Boni-Mitake, M., Costa, H., Spencer, P. J., Vassilieff, V. S. & Rogero, J. R. (2001). *Braz. J. Med. Biol. Res.* **34**, 1531–1538.

Bontems, F., Gilquin, B., Roumestand, C., Ménez, A. & Toma, F. (1992). *Biochemistry*, **31**, 7756–7764.

Carvalho, A. de O. & Gomes, V. M. (2009). *Peptides*, **30**, 1007–1020.

Cociancich, S., Ghazi, A., Hetru, C., Hoffmann, J. A. & Letellier, L. (1993). *J. Biol. Chem.* **268**, 19239–19245.

Cornet, B., Bonmatin, J.-M., Hetru, C., Hoffmann, J. A., Ptak, M. & Vovelle, F. (1995). *Structure*, **3**, 435–448.

Coronado, M. A., Georgieva, D., Buck, F., Gabdoulkhakov, A. H., Ullah, A., Spencer, P. J., Arni, R. K. & Betzel, C. (2012). *Acta Cryst.* F**68**, 1052–1054.

Dimarcq, J.-L., Bulet, P., Hetru, C. & Hoffmann, J. (1998). *Biopolymers*, **47**, 465–477.

Emsley, P., Lohkamp, B., Scott, W. G. & Cowtan, K. (2010). *Acta Cryst.* D**66**, 486–501.

Endo, T., Oya, M., Ozawa, H., Kawano, Y., Giglio, J. R. & Miyazawa, T. (1989). *Protein Chem.* **8**, 807–815.

Fadel, V., Bettendorff, P., Herrmann, T., de Azevedo, W. F., Oliveira, E. B., Yamane, T. & Wüthrich, K. (2005). *Toxicon*, **46**, 759–767.

Ganz, T. (2003). *Nature Rev. Immunol.* **3**, 710–720.

Ganz, T. (2004). *J. Leukoc. Biol.* **75**, 34–38.

Ganz, T., Selsted, M. E., Szklarek, D., Harwig, S. S., Daher, K., Bainton, D. F. & Lehrer, R. I. (1985). *J. Clin. Invest.* **76**, 1427–1435.

Gasteiger, E., Hoogland, C., Gattiker, A., Duvaud, S., Wilkins, M. R., Appel, R. D. & Bairoch, A. (2005). *The Proteomics Protocols Handbook*, edited by J. M. Walker, pp. 571–607. Totowa: Humana Press.

Giorgi, R., Bernardi, M. M. & Cury, Y. (1993). *Toxicon*, **10**, 1257–1265.

Gonçalves, J. M. & Polson, A. (1947). *Arch. Biochem.* **13**, 253–259.

Hoover, D. M., Chertov, O. & Lubkowski, J. (2001). *J. Biol. Chem.* **276**, 39021–39026.

Hoover, D. M., Rajashankar, K. R., Blumenthal, R., Puri, A., Oppenheim, J. J., Chertov, O. & Lubkowski, J. (2000). *J. Biol. Chem.* **275**, 32911–32918.

Huang, R.-H., Xiang, Y., Tu, G.-Z., Zhang, Y. & Wang, D.-C. (2004). *Biochemistry*, **43**, 6005–6012.

Kabsch, W. (2010). *Acta Cryst.* D**66**, 125–132.

Kerkis, A., Kerkis, I., Rádis-Baptista, G., Oliveira, E. B., Vianna-Morgante, A. M., Pereira, L. V. & Yamane, T. (2004). *FASEB J.* **18**, 1407–1409.

Kerkis, I., Silva, F. de S., Pereira, A., Kerkis, A. & Rádis-Baptista, G. (2010). *Expert Opin. Investig. Drugs*, **19**, 1515–1525.

Lamberty, M., Caille, A., Landon, C., Tassin-Moindrot, S., Hetru, C., Bulet, P. & Vovelle, F. (2001). *Biochemistry*, **40**, 11995–12003.

Landon, C., Cornet, B., Bonmatin, J. M., Kopeyan, C., Rochat, H., Vovelle, F. & Ptak, M. (1996). *Eur. J. Biochem.* **236**, 395–404.

Lee, J.-Y., Choi, Y.-S., Suh, J.-S., Kwon, Y.-M., Yang, V. C., Lee, S.-J., Chung, C.-P. & Park, Y.-J. (2011). *Int. J. Cancer*, **128**, 2470–2480.

Lehrer, R. I., Lichtenstein, A. K. & Ganz, T. (1993). *Annu. Rev. Immunol.* **11**, 105–128.

Mancin, A. C., Soares, A. M., Andrião-Escarso, S. H., Faça, V. M., Greene, L. J., Zuccolotto, S., Pelá, I. R. & Giglio, J. R. (1998). *Toxicon*, **36**, 1927–1937.

Murshudov, G. N., Skubák, P., Lebedev, A. A., Pannu, N. S., Steiner, R. A., Nicholls, R. A., Winn, M. D., Long, F. & Vagin, A. A. (2011). *Acta Cryst.* D**67**, 355–367.

Nicastro, G., Franzoni, L., de Chiara, C., Mancin, A. C., Giglio, J. R. & Spisni, A. (2003). *Eur. J. Biochem.* **270**, 1969–1979.

Oguiura, N., Boni-Mitake, M., Affonso, R. & Zhang, G. (2011). *J. Antibiot.* **64**, 327–331.

Petoukhov, M. V., Konarev, P. V., Kikhney, A. G. & Svergun, D. I. (2007). *J. Appl. Cryst.* **40**, s223–s228.

Ponce-Soto, L. A., Martins-de-Souza, D., Martins, D., Novello, J. C. & Marangoni, S. (2007). *Protein J.* **26**, 533–540.

Schibli, D. J., Hunter, H. N., Aseyev, V., Starner, T. D., Wiencek, J. M., McCray, P. B., Tack, B. F. & Vogel, H. J. (2002). *J. Biol. Chem.* **277**, 8279–8289.

Sverdlova, A. N. & Nefelova, M. V. (1999). *Mol. Gen. Mikrobiol. Virusol.*, pp. 34–40.

Torres, A. M., de Plater, G. M., Doverskog, M., Birinyi-Strachan, L. C., Nicholson, G. M., Gallagher, C. H. & Kuchel, P. W. (2000). *Biochem. J.* **348**, 649–656.

Toyama, M. H., Carneiro, E. M., Marangoni, S., Barbosa, R. L., Corso, G. & Boschero, A. C. (2000). *Biochim. Biophys. Acta*, **1474**, 56–60.

Yount, N. Y., Kupferwasser, D., Spisni, A., Dutz, S. M., Ramjan, Z. H., Sharma, S., Waring, A. J. & Yeaman, M. R. (2009). *Proc. Natl Acad. Sci. USA*, **106**, 14972–14977.